Supporting Information (SI) *for:*

Inducing the Metal Support Interaction and Enhancing the Ammonia Synthesis Activity of Ceria-supported Ruthenium Catalyst via N_2H_4 Reduction

Chunyan Li[†], Fangming Liu[†], Yuying Shi[†], Yiping Zheng[†], Biyun Fang[†], Jianxin Lin[†], Jun Ni[†], Xiuyun Wang[†], Bingyu Lin*[, †], Lilong Jiang*[, †]

[†]National Engineering Research Center of Chemical Fertilizer Catalyst, College of Chemical Engineering, Fuzhou University, Fuzhou 350002, Fujian, China

*E-mail: bylin@fzu.edu.cn (Bingyu Lin)

*E-mail: jll@fzu.edu.cn (Lilong Jiang)

Number of pages: 22
Number of figures: 10
Number of tables: 4

Characterization

Inductively coupled plasma-optical emission spectroscopy (ICP–OES) was analyzed by OPTIMA 8000 (Perkin - Elmer). Transmission electron microscopy (TEM) and high-angle annular dark-field scanning transmission electron microscopy (HAADF-STEM) images were obtained by a FEI Tecnai G2 F30 microscope. The Brunauer–Emmett–Teller (BET) surface area, pore volume, and pore size distribution of the samples were measured with an ASAP 2020M instrument using adsorption of N_2 at 77 K. Prior to adsorption analysis, the catalysts were degassed in a flowing N_2 at 300 °C for 3 h. The phase purity and crystal structure of the catalysts were examined by X-ray diffraction (XRD, PANalytical X'Pert3 Powder diffractometer), using Cu Kα radiation (λ=0.154 32 nm). Raman spectra of samples were acquired on an InVia Reflex Raman microscope equipped with a 532 nm laser. UV–vis spectra were recorded on a UV–vis spectrometer (Lambda 950) with 650 nm wavelength. As white standard, MgO powder was employed in the same geometry as the sample.

Diffuse reflectance infrared Fourier transform spectroscopy (DRIFTS) was measured on a Nicolet 6700 spectrometer operated at a resolution of 4 cm^{-1} with 32 scans. For CO adsorption measurements, For CO adsorption measurements of fresh catalysts, the samples were reduced in hydrogen at 500 °C for 6 h, then purged with He and cooled down to 50 °C. After the collection of background spectrum, the sample was exposed to 5% CO/He (50 mL/min) for 10 min. To acquire the information related to deuterium species, the sample was reduced at 500 °C in H_2 and then cooled down to 50 °C in a flow of He. After collection of background spectrum, the sample was exposed to D_2 for 10 min and the spectra was collected.

Hydrogen temperature-programmed reduction (H_2-TPR) of as-prepared catalysts was carried out on a Micromeritics AutoChem II 2920. The catalyst (100 mg, sieve fraction 0.30–0.56 mm) was pretreated in Ar at 150 °C for 60 min and then cooled to 50 °C. Afterward, the samples were heated in a flow of 10% H_2/Ar mixture (30 mL min^{-1}) to 600 °C at a rate of 10 °C min^{-1}. Temperature-programmed desorption

(TPD) experiment was also performed using the same AutoChem II 2920 equipment. A sample (100 mg) was reduced in H_2 at 500 °C for 6 h, and then purged with Ar and cooled to 400 °C. Afterwards, the gas flow was switched to pure H_2 for sample exposure at 400 °C for 1 h. After cooling to 50 °C, the sample was purged with Ar for 1 h, and then heated to 600 °C at a rate of 10 °C/min. A Hiden Analytical HPR-20 mass spectrometer was used to monitor the water (m/z=18) and hydrogen (m/z=2) signals. Carbon monoxide temperature-programmed reduction (CO-TPR) was performed using the same AutoChem II 2920 instrument. The fresh sample was exposed to H_2 at 500 °C for 2 h, and then cooled to 50 °C. Afterwards, carbon monoxide was introduced, and the sample was heated from 50 °C to 900 °C at a rate of 10 °C/min. The mass signals were obtained by a HPR-20 mass spectrometer.

Temperature-programmed surface reaction (TPSR) measurement was carried out on the same AutoChem II 2920 instrument. The reduced sample was exposed to D_2 or N_2 at 400 °C for 1 h, and then cooled to 50 °C in the gas selected for exposure. Finally, the feed gas was switched to a 3.3%N_2−10%H_2−Ar mixture, and the catalyst was heated to 600 °C.

Mass and Heat Transfer Calculations for Ammonia Synthesis over Ru/CeO_2-N_2H_4

Mass and Heat Transfer Calculations for Ammonia Synthesis on Ru/CeO_2-N_2H_4

Mears Criterion for External Diffusion (Fogler, p841; Mears, 1971)

If $\frac{-r_A' \rho_b R n}{k_c C_{Ab}} < 0.15$, then external mass transfer effects can be neglected. (S1)

$-r_A'$ = reaction rate of nitrogen, kmol/kg-cat·s

n = reaction order with respect to N_2 (*e.g.* K. Aika et al, Appl. Catal., **28**(1986) 57–68).

R = catalyst particle radius, m

ρ_b = bulk density of catalyst bed, kg/m^3

C_{Ab} = bulk gas concentration of nitrogen, kmol/m^3

k_c = mass transfer coefficient, m/s

$\frac{-r_A' \rho_b Rn}{k_c C_{Ab}}$ = [3.1 x 10^{-8} kmol-N_2/kg-cat·s] [910 kg/m^3][3 x 10^{-4} m][1]/([1.7 m/s]*[0.045 kmol/m^3])= **1.1x10^{-7} <0.15.**

Weisz-Prater Criterion for Internal Diffusion for Ammonia Synthesis over Ru/CeO_2-N_2H_4

If $C_{WP} = \frac{-r'_A \rho_c R^2}{D_e C_{Ab}} < 1$, the internal mass transfer effects can be neglected. (S2)

$-r_A'$ = reaction rate of nitrogen, kmol /(kg_{cat}·s)

ρ_c = solid catalyst density (kg m^{-3})

R = catalyst particle radius, m

ρ_b = bulk density of catalyst bed, kg/m^3

C_{Ab} = bulk gas concentration of nitrogen, kmol/m^3

k_c = mass transfer coefficient, m/s

D_e = effective gas-phase diffusivity, m^2/s

$C_{WP} = \frac{-r'_A \rho_c R^2}{D_e C_{Ab}}$ = [3.1 x 10^{-8} kmol-N_2/kg-cat·s] × [4×10^3 kg-cat/m^3] × [3 x 10^{-4} m]^2 / ([3.34 x 10^{-6} m^2/s] × [0.045 kmol/m^3]) = **7.4x10^{-5} < 1**

Mears Criterion for External (Interphase) Heat Transfer for Ammonia Synthesis over Ru/CeO_2-N_2H_4

$$\left| \frac{-\Delta H_r (-r_A') \rho_b R E}{h_t T_b^{\,2} R_g} \right| < 0.15 \quad \text{(S3)}$$

[136.9 kJ/mol× 3.1 x 10^{-8} kmol-N_2/(kg-cat·s) × 910 kg-cat/m^3 ×3 x 10^{-4} m× 150 kJ/mol] / [185.3 kJ/m^2.K.s × 673^2 K^2× 8.314 ×10^{-3} kJ/mol.K]= 2.5x10^{-7} < 0.15

Mears Criterion for Combined Interphase and Intraparticle Heat and Mass Transport for Ammonia Synthesis over Ru/CeO_2-N_2H_4

$$\frac{-r'_A R^2}{C_{Ab} D_e} < \frac{1+0.33\gamma\chi}{\left|n-\gamma_b\beta_b\right|\left(1+0.33n\omega\right)} \tag{S4}$$

$$\gamma = \frac{E}{R_g T_s} \tag{S5}$$

$$\gamma_b = \frac{E}{R_g T_b} \tag{S6}$$

$$\beta_b = \frac{\left(-\Delta H_r\right) D_e C_{Ab}}{\lambda T_b} \tag{S7}$$

$$\chi = \frac{\left(-\Delta H_r\right) - r'_A R}{h_t T_b} \tag{S8}$$

$$\omega = \frac{-r'_A R}{k_c C_{Ab}} \tag{S9}$$

γ = Arrhenius number; β_b = heat generation function;

λ = catalyst thermal conductivity, W/m.K;

χ = Damköhler number for interphase heat transport

ω = Damköhler number for interphase mass transport

$\frac{-r'_A \rho_b R^2}{C_{Ab} D_e}$ = [3.1 x 10^{-8} kmol-N_2/kg-cat·s × 910 kg-cat/m^3× (3 x 10^{-4})^2 m^2]/ ([3.34 x 10^{-6} m^2/s] × [0.045 kmol/m^3]) = 1.7x10^{-5}

$\frac{1+0.33\gamma\chi}{\left|n-\gamma_b\beta_b\right|\left(1+0.33n\omega\right)}$ =2.25

Left member < Right member

Table S1 Catalytic performance of Ru-based catalysts on various supports.

Samples	Rate (μmol g^{-1} h^{-1})	TOF [a] (Ru $atom^{-1}$ s^{-1})	Reaction conditions	SV (mL g^{-1} h^{-1})	Ref.
Ru/CeO_2-H_2	3987	11.3×10^{-3}	1MPa, 400 °C	36 000	This
Ru/CeO_2-N_2H_4	5521	15.6×10^{-3}	1MPa, 400 °C	36 000	work
Ba-Ru/Al_2O_3	2796	1.7×10^{-3}	1MPa, 400 °C	36 000	1
Ba-Ru/Al_2O_3	2083	1.3×10^{-3}	1MPa, 400 °C	18 000	1
Ru/Ti-Ce-S	14 580	14.1×10^{-3}	1MPa, 400 °C	36 000	2
Ru/CeO_2	4394	4.2×10^{-3}	1MPa, 400 °C	36 000	2
Ru/TiO_2	836	8.0×10^{-4}	1MPa, 400 °C	36 000	2
Ru/TiO_2-anatase	324	3.1×10^{-4}	1MPa, 400 °C	36 000	2
Ru/TiO_2-rutile	530	5.1×10^{-4}	1MPa, 400 °C	36 000	2
Ru(10%)/Ba-$Ca(NH_2)_2$	60 400	16.9×10^{-3}	0.9MPa,360°C	36 000	3
	50 000	14.0×10^{-3}	0.9MPa,400°C	36 000	
Ru(6%)-Cs/MgO	23 000	6.5×10^{-3}	0.9MPa,400°C	36 000	3
Ru(9.1%)-Ba/AC	8285	2.6×10^{-3}	1 MPa, 400 °C	18 000	4
Ru(6%)-Cs/MgO	12 117	5.7×10^{-3}	1 MPa, 400 °C	18 000	4
Ru(4%)/C12A7:e^-	6089	4.3×10^{-3}	1 MPa, 400 °C	18 000	4
Ru(5%)/CeO_2	7200	4.0×10^{-3}	0.9MPa,400°C	18 000	5
Ru(5%)/MgO	1800	1.0×10^{-3}	0.9MPa,400°C	18 000	5
Ru(7.8%)/Y5Si3	4100	1.5×10^{-3}	1 MPa, 400 °C	18 000	6
Ru(4%)/r-CeO_2	3830	2.7×10^{-3}	1 MPa, 400 °C	18 000	7

Ru(4%)/c-CeO_2	1289	0.9×10^{-3}	1 MPa, 400 °C	18 000	7
Ru(4%)/p-CeO_2	529	0.4×10^{-3}	1 MPa, 400 °C	18 000	7
Ru(5%)/$La_{0.5}Ce_{0.5}O_{1.75}$	65 000	36.5×10^{-3}	1 MPa, 400 °C	72 000	8
Cs-Ru(1%)/MgO	2700	1.0×10^{-3}	5 MPa, 400 °C	66 000	9
Ru(1%)/$BaTiO_3$	4100	1.5×10^{-3}	5 MPa, 400 °C	66 000	9
Ba-Ru/Al_2O_3-980	7217	4.5×10^{-3}	1 MPa, 400 °C	60 000	10
Ba-Ru/gC-Al_2O_3	4219	2.6×10^{-3}	1 MPa, 400 °C	18 000	1

[a] based on total number of Ru atoms

Table S2 The amount of Ru species and textural properties of CeO_2 and Ru catalysts

Samples	Ru (wt%) [a]	Surface area (m^2/g^{-1})	Pore volume (cm^3g^{-1})	Average pore size (nm)
CeO_2	--	18	0.04	13
Ru/CeO_2-H_2	0.985	20	0.05	16
Ru/CeO_2-N_2H_4	0.966	58	0.34	26

[a] obtained by ICP analysis.

Table S3 CO chemisorption of Ru catalysts

Samples	V_{CO} (ml g^{-1})	D_{CO} (%) [a]	amount of exposed surface Ru atoms (μmol g^{-1})[a]
Ru/CeO_2-H_2	0.5	23.2	22.3
Ru/CeO_2-N_2H_4	1.1	49.8	49.1

[a] Determined by CO chemisorption, assuming a stoichiometry of Ru/CO = 1.

Table S4 H_2 consumption during the H_2-TPR measurements over the Ru catalysts.

Samples	Theoretical H_2 consumption ($ml\ g^{-1}$) [a]	H_2 consumption of the as-prepared catalyst ($ml\ g^{-1}$)		H_2 consumption of the oxidized catalyst ($ml\ g^{-1}$)	
		α (<163 °C)	β (>163 °C)	α (<163 °C)	β (>163 °C)
Ru/CeO_2-H	4.4	1.2	0.6	0.2	0.02
Ru/CeO_2-N_2H_4	4.4	1.7	1.1	0.5	0.05

[a] Theoretical H_2 consumption for Ru reduction of Ru catalysts.

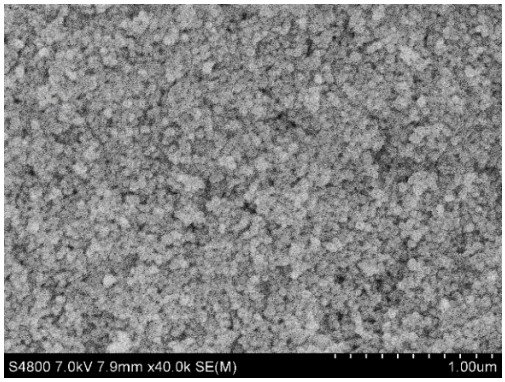

Figure S1 The SEM image of CeO_2.

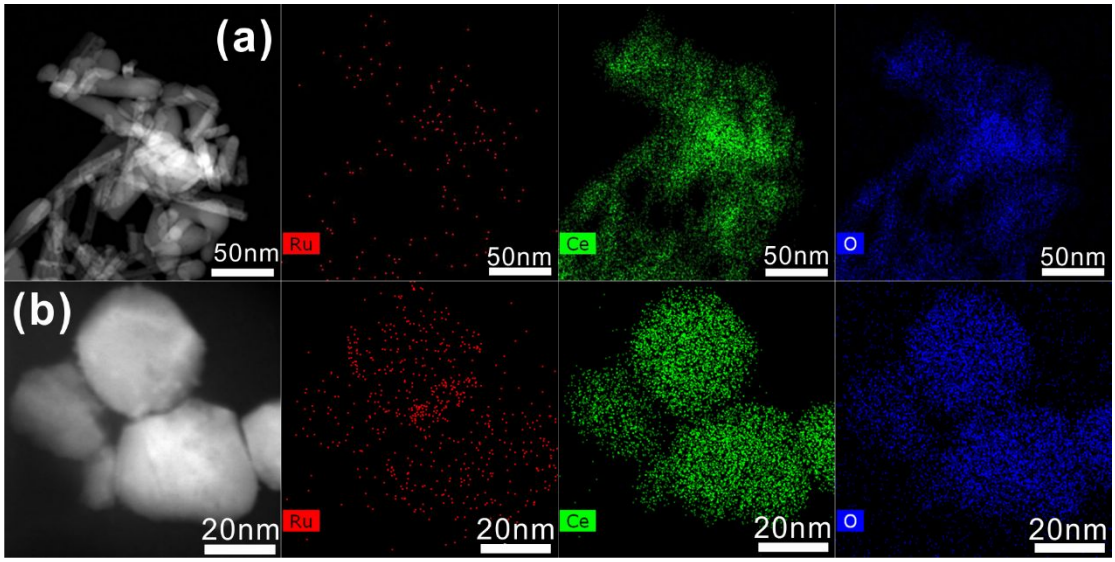

Figure S2 HAADF-STEM image and the corresponding element maps of Ru catalysts (a) Ru/CeO_2-N_2H_4 and (b) Ru/CeO_2-H_2.

.

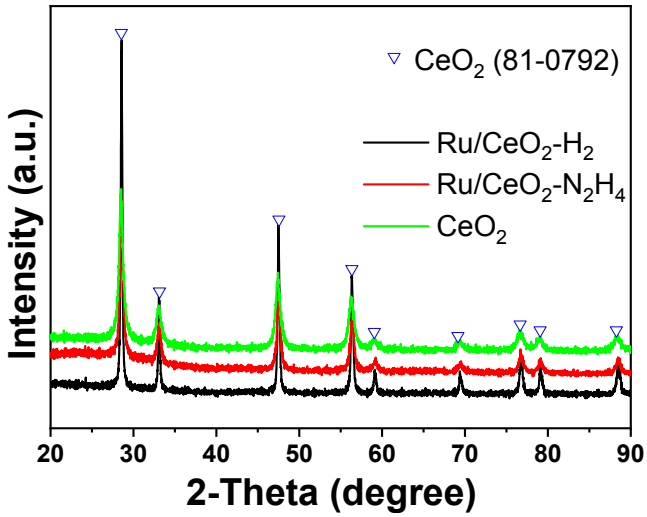

Figure S3 XRD patterns of CeO_2 and Ru/CeO_2 catalysts.

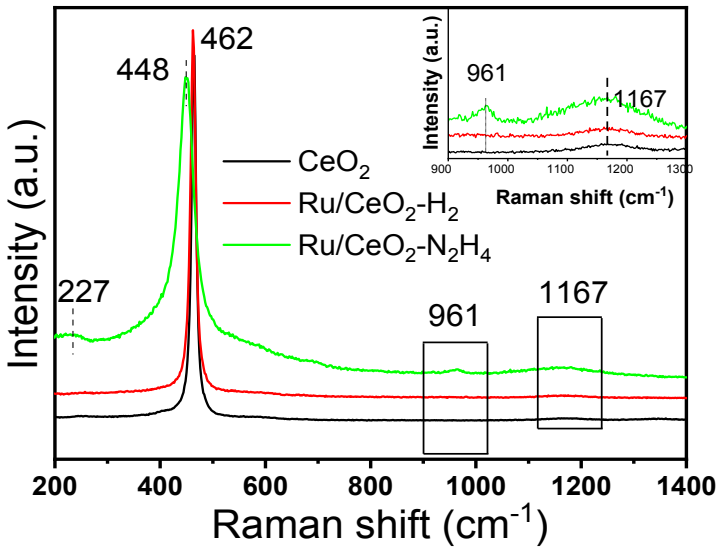

Figure S4 Raman spectra for CeO_2 support and Ru/CeO_2 samples.

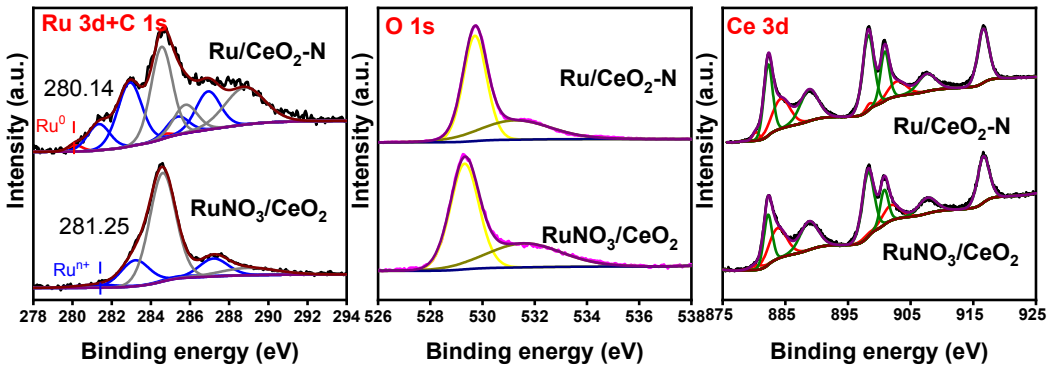

Figure S5 XPS Ru 3d, Ce 3d and O 1s spectra of $RuNO_3/CeO_2$ (the untreated sample) and Ru/CeO_2-N.

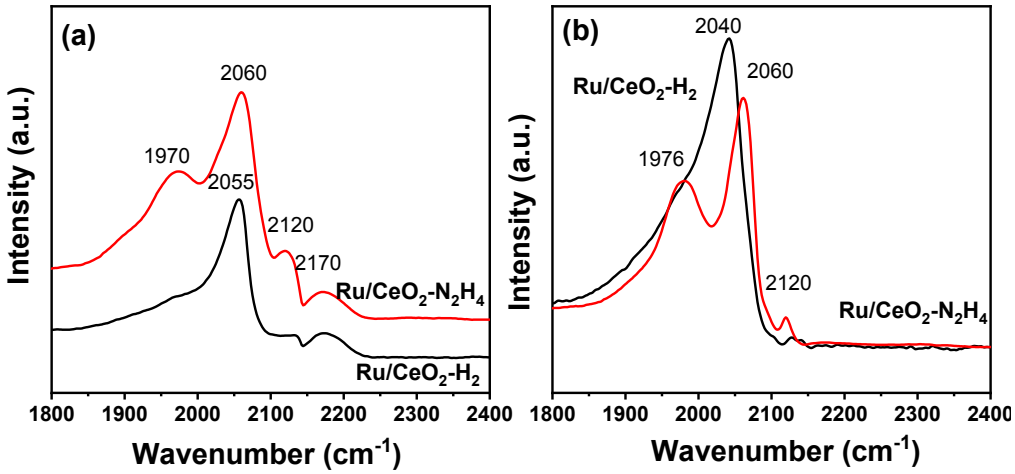

Figure S6 In situ DRIFT spectra of (a) CO adsorption saturated over Ru catalysts at 50 °C (b) after 10 min He purging.

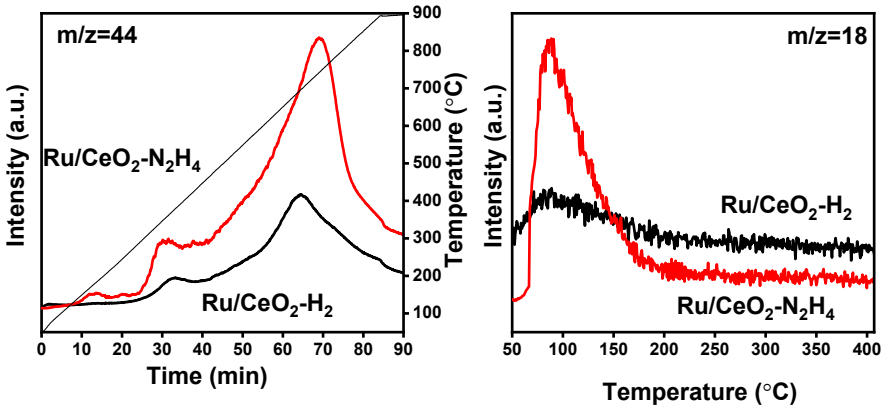

Figure S7 The mass signals of CO_2 and H_2O obtained from CO-TPR study of the Ru catalysts.

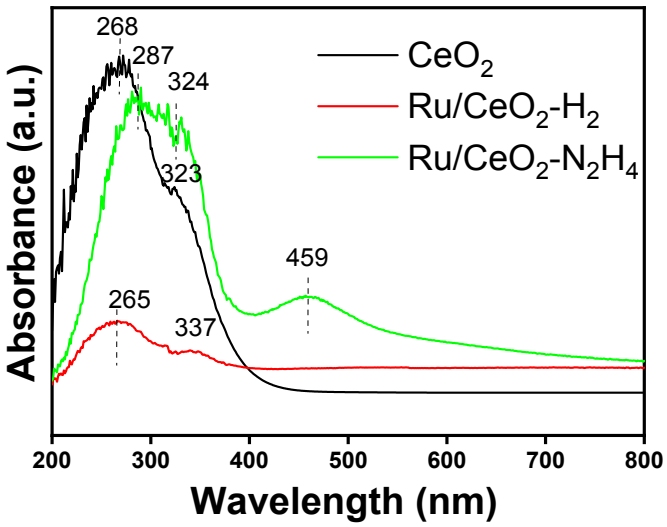

Figure S8 UV-Vis spectra of CeO_2 and Ru catalysts.

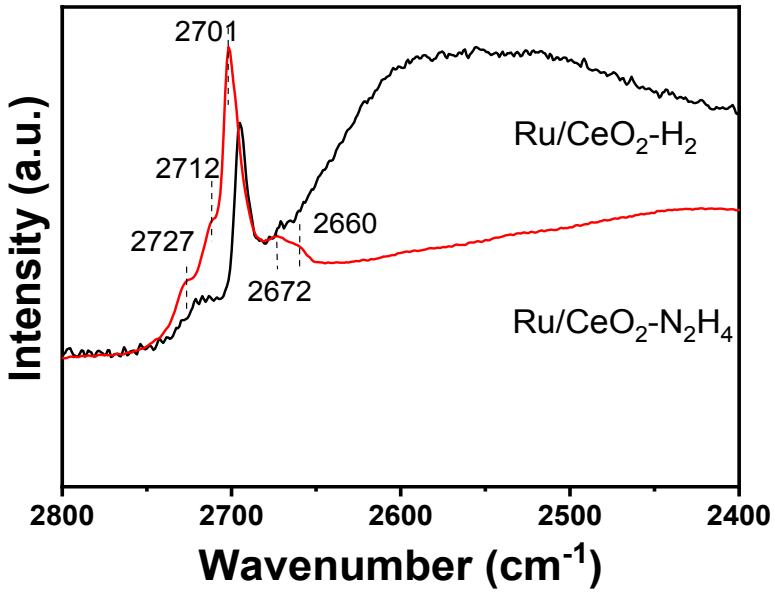

Figure S9 DRIFTS spectra collected after exposure to D_2 for 10 min at 50 °C

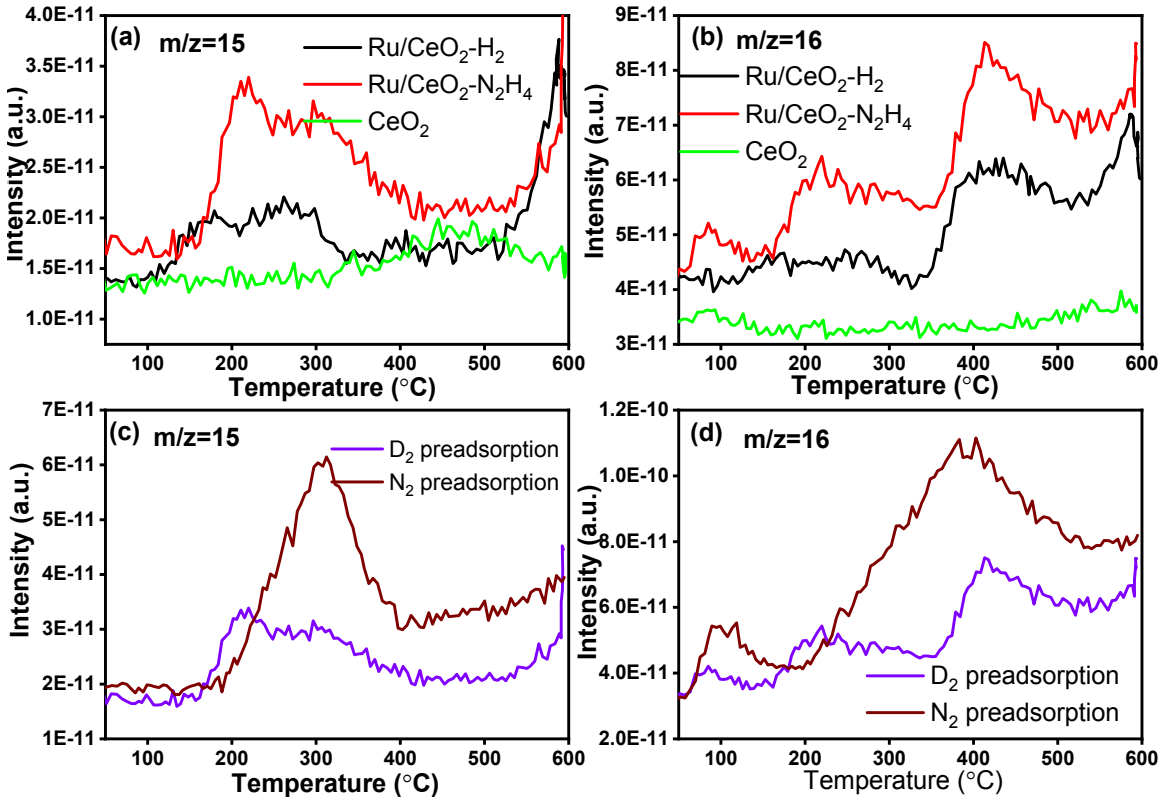

Figure S10 The signals of m/z=15 (NH) and m/z=16 (NH_2 or ND) versus temperature detected by mass spectrometry during TPSR study in 3.3%N_2−10%H_2−Ar mixture (a) and (b) D_2 preadsorption of various samples, (c) and (d) different atmospheres Pre-adsorption over Ru/CeO_2-N_2H_4.

References

(1) Lin, B.; Heng, L.; Yin, H.; Fang, B.; Ni, J.; Wang, X.; Lin, J.; Jiang, L., Effects of Using Carbon-Coated Alumina as Support for Ba-Promoted Ru Catalyst in Ammonia Synthesis. *Ind. Eng. Chem. Res.* **2019,** *58* (24), 10285-10295.

(2) Wu, Y.; Li, C.; Fang, B.; Wang, X.; Ni, J.; Lin, B.; Lin, J.; Jiang, L., Enhanced ammonia synthesis performance of ceria-supported Ru catalysts via introduction of titanium. *Chem. Commun.* **2020,** *56* (7), 1141-1144.

(3) Kitano, M.; Inoue, Y.; Sasase, M.; Kishida, K.; Kobayashi, Y.; Nishiyama, K.; Tada, T.; Kawamura, S.; Yokoyama, T.; Hara, M.; Hosono, H., Self-organized Ruthenium–Barium Core–Shell Nanoparticles on a Mesoporous Calcium Amide Matrix for Efficient Low-Temperature Ammonia Synthesis. *Angew. Chem. Int. Ed.* **2018,** *57* (10), 2648–2652.

(4) Kitano, M.; Inoue, Y.; Yamazaki, Y.; Hayashi, F.; Kanbara, S.; Matsuishi, S.; Yokoyama, T.; Kim, S.-W.; Hara, M.; Hosono, H., Ammonia synthesis using a stable electride as an electron donor and reversible hydrogen store. *Nat. Chem.* **2012,** *4* (11), 934–940.

(5) Sato, K.; Imamura, K.; Kawano, Y.; Miyahara, S.-i.; Yamamoto, T.; Matsumura, S.; Nagaoka, K., A low-crystalline ruthenium nano-layer supported on praseodymium oxide as an active catalyst for ammonia synthesis. *Chem. Sci.* **2017,** *8* (1), 674–679.

(6) Lu, Y.; Li, J.; Tada, T.; Toda, Y.; Ueda, S.; Yokoyama, T.; Kitano, M.; Hosono, H., Water Durable Electride Y_5Si_3: Electronic Structure and Catalytic Activity for Ammonia Synthesis. *J. Am. Chem. Soc.* **2016,** *138* (12), 3970–3973.

(7) Ma, Z.; Zhao, S.; Pei, X.; Xiong, X.; Hu, B., New insights into the support morphology-dependent ammonia synthesis activity of Ru/CeO_2 catalysts. *Catal. Sci. Technol.* **2017,** *7* (1), 191-199.

(8) Ogura, Y.; Sato, K.; Miyahara, S.-i.; Kawano, Y.; Toriyama, T.; Yamamoto, T.; Matsumura, S.; Hosokawa, S.; Nagaoka, K., Efficient ammonia synthesis over a $Ru/La_{0.5}Ce_{0.5}O_{1.75}$ catalyst pre-reduced at high temperature. *Chem. Sci.* **2018,** *9* (8), 2230–2237.

(9) Kobayashi, Y.; Tang, Y.; Kageyama, T.; Yamashita, H.; Masuda, N.; Hosokawa, S.; Kageyama, H., Titanium-Based Hydrides as Heterogeneous Catalysts for Ammonia Synthesis. *J. Am. Chem. Soc.* **2017,** *139* (50), 18240–18246.

(10) Lin, B.; Heng, L.; Fang, B.; Yin, H.; Ni, J.; Wang, X.; Lin, J.; Jiang, L., Ammonia Synthesis Activity of Alumina-Supported Ruthenium Catalyst Enhanced by Alumina Phase Transformation. *ACS Catal.* **2019,** *9* (3), 1635–1644.